

**MODIFICATION OF DYE-SENSITIZED SOLAR
CELLS: EFFECT OF METAL-ORGANIC
FRAMEWORK-DERIVED TIN DIOXIDE TO
TITANIA PHOTOANODE**

CHEONG VON FEI



**UNIVERSITY OF MALAYA
UMS**
UNIVERSITI MALAYSIA SABAH

**THIS IS SUBMITTED IN FULFILLMENT FOR
THE DEGREE OF MASTER OF SCIENCE**

**FACULTY OF SCIENCE AND NATURAL
RESOURCES
UNIVERSITI MALAYSIA SABAH
2017**

UNIVERSITI MALAYSIA SABAH

BORANG PENGESAHAN TESIS

JUDUL : _____

IJAZAH : _____

SAYA : _____ SESI PENGAJIAN : _____

(HURUF BESAR)

Mengaku membenarkan tesis *(LPSM/Sarjana/Doktor Falsafah) ini disimpan di Perpustakaan Universiti Malaysia Sabah dengan syarat-syarat kegunaan seperti berikut:-

1. Tesis adalah hak milik Universiti Malaysia Sabah.
2. Perpustakaan Universiti Malaysia Sabah dibenarkan membuat salinan untuk tujuan pengajian sahaja.
3. Perpustakaan dibenarkan membuat salinan tesis ini sebagai bahan pertukaran antara institusi pengajian tinggi.
4. Sila tandakan (/)

SULIT

(Mengandungi maklumat yang berdarjah keselamatan atau kepentingan Malaysia seperti yang termaktub di AKTA RAHSIA RASMI 1972)

TERHAD

(Mengandungi maklumat TERHAD yang telah ditentukan oleh organisasi/badan di mana penyelidikan dijalankan)

TIDAK TERHAD

Disahkan oleh:

(TANDATANGAN PENULIS)

Alamat Tetap: _____

TARIKH: _____

(TANDATANGAN PUSTAKAWAN)_____
(NAMA PENYELIA)

TARIKH: _____

Catatan:

*Potong yang tidak berkenaan.

*Jika tesis ini SULIT dan TERHAD, sila lampirkan surat daripada pihak berkuasa/organisasi berkenaan dengan menyatakan sekali sebab dan tempoh tesis ini perlu dikelaskan sebagai SULIT dan TERHAD.

*Tesis dimaksudkan sebagai tesis bagi Ijazah Doktor Falsafah dan Sarjana Secara Penyelidikan atau disertai bagi pengajian secara kerja kursus dan Laporan Projek Sarjana Muda (LPSM).

DECLARATION

I hereby declare that the material in this thesis is my own except for quotations, excerpts, equations, summaries and references, which have been duly acknowledged.

13 September 2017

Cheong Von Fei
MS1421085T



UMS
UNIVERSITI MALAYSIA SABAH

CERTIFICATION

NAME : **CHEONG VON FEI**
MATRIC NO. : **MS1421085T**
TITLE : **MODIFICATION OF DYE-SENSITIZED SOLAR CELLS:
EFFECT OF METAL-ORGANIC FRAMEWORK-
DERIVED TIN DIOXIDE TO TITANIA
PHOTOANODE**
DEGREE : **MASTER OF SCIENCE
(INDUSTRIAL CHEMISTRY)**
VIVA DATE : **12 SEPTEMBER 2017**



CERTIFIED BY

UMS
UNIVERSITI MALAYSIA SABAH

SIGNATURE

2. CO-SUPERVISOR

Assoc. Prof. Dr. Rachel Fran Mansa

ACKNOWLEDGEMENTS

I would like to express my deepest gratitude and appreciation to my supervisor Dr. Moh Pak Yan for his guidance, patience, support and constructive feedback towards my work. I also wish to thank my co-supervisor Dr. Rachel Fran Mansa for her guidance and advice.

Special thanks to Dr. Rachel's research group members, Liow Kai Sing, Stephanie Lau and Michelle Ung for their assistance in solar cell characterization. Also thanks to my seniors, Suzanna, Wafa, Hasmira, and Hadi for a joyful company in green chemistry laboratory.

Besides, I would like to thank Mr. Taipin for his assistance in natural product laboratory and Mr. Abdul Rahim for his help in performing X-ray diffractometry (XRD). I would also like to express my gratitude to Mr. Farhan and Mr. Afifi at Borneo Tropical and Conservation Institute (IBTP) for their assistance in using scanning electron microscope (SEM).

I wish to express my special thanks to Prof. Mohammad B. Kassim, Dr. Lorna Jeffry, and Mr. Ng Kim Hang for assisting me in UKM for solar cell characterization. In addition, I would like to thank Ministry of Higher Education, Malaysia (MOHE) for the provision of grant through Trans Disciplinary Research Grant Scheme (TRGS0001-SG-2/2014).

I would like to thank my best friends, Teo Szea Err, Puah Perng Yang, Chai Wui Hung, and Quek Kye Shane for assisting and encouraging me throughout my master degree.

Last but not least, I would like to thank my family members for their continuous love and support during my master degree. I would like to take the opportunity to offer my deepest compliments to my parents for their love and contributions into my life. I am also thankful to my younger brother for his wishes and support.

Cheong Von Fei
13 September 2017

ABSTRACT

Dye-sensitized solar cells (DSSCs) have been considered as a promising alternative to conventional silicon-based solar cells due to their low production cost, simple fabrication process, and high efficiency. However, the best power conversion efficiency reported for DSSCs to date is only 12%, which is far lower than that of conventional solar cells (26%). In this study, metal-organic framework-derived SnO₂ was loaded into the TiO₂ photoanode to improve the overall photovoltaic performance of DSSCs. The as-synthesized SnO₂ powder with weight ratios of 10, 25, 50, and 75 wt% was mixed with commercial TiO₂ followed by casting the mixture on a FTO glass through doctor-blade method. The Sn-MOF-derived SnO₂/TiO₂ materials were confirmed using PXRD while its chemical functionality of SnO₂/TiO₂ photoanodes was identified using FTIR. SEM images of the photoanodes showed that the Sn-MOF-derived SnO₂ was well-loaded into the TiO₂. The power conversion efficiency of Sn-MOF-derived SnO₂/TiO₂ DSSCs with an active area of 0.25 cm² was evaluated using potentiostat under illumination of 60 mW cm⁻². The DSSC assembled using SnO₂/TiO₂ (1:9) photoanode delivered the best power conversion efficiency i.e. 3.57%. The efficiency of SnO₂/TiO₂ (1:9) based DSSC is lower than that of TiO₂ alone (4.09%). This was attributed to its higher recombination rate as a result of the lower conduction band edge of SnO₂ with respect to TiO₂. However, its efficiency is 2 and 71 times higher than that of the Sn-MOF-derived SnO₂ alone (1.61%) and Sn-MOF alone (0.05%), respectively. Dye loading of the photoanodes revealed that SnO₂/TiO₂ (1:9) photoanode has the highest dye adsorption capacity among the photoanodes with a concentration of 9.14×10^{-8} mol cm⁻². This implies that Sn-MOF-derived SnO₂/TiO₂ photoanode can perform better than that of TiO₂ alone if the recombination in the device can be suppressed. This study provides a new insight into the fabrication of photoanode of high performance DSSC devices.

ABSTRAK

Pengubahsuaian Sel Surya Terpeka Pewarna: Kesan Timah Dioksida daripada Kerangka Logam-Organik ke Titania Fotoanod

Sel suria terpeka pewarna (DSSC) telah dianggap sebagai pengganti yang baik kepada sel suria tradisional berasaskan silikon kerana kos pembuatan yang rendah, proses pembuatan yang mudah, dan kecekapan yang tinggi. Walau bagaimanapun, kecekapan penukaran kuasa yang tertinggi dilaporkan untuk DSSC setakat ini hanya 12%, jauh lebih rendah berbanding dengan sel suria tradisional (26%). Dalam kajian ini, SnO₂ daripada kerangka logam-organik berasaskan timah telah ditambahkan ke dalam fotoanod TiO₂ untuk meningkatkan prestasi fotovoltai keseluruhan DSSC. Serbuk SnO₂ diperolehi dengan nisbah berat 10, 25, 50, dan 75% telah dicampur dengan TiO₂ komersial, diikuti dengan penyalutan campuran ini pada kaca FTO melalui kaedah doctor-blade. Bahan SnO₂/TiO₂ yang diperolehi telah disahkan menggunakan PXRD, manakala kumpulan berfungsi bagi fotoanod SnO₂/TiO₂ (1:9) telah dikenal pasti menggunakan FTIR. Imej SEM bagi fotoanod menunjukkan bahawa SnO₂ telah berjaya digaulkan ke dalam TiO₂. Kecekapan penukaran kuasa bagi DSSC berasaskan SnO₂/TiO₂ dengan keluasan aktif 0.25 cm² telah dinilai menggunakan potentiostat di bawah penyinaran 60 mW cm⁻². DSSC berasaskan fotoanod SnO₂/TiO₂ (1:9) memberikan kecekapan penukaran kuasa terbaik iaitu sebanyak 3.57%. Kecekapan DSSC berasaskan SnO₂/TiO₂ (1:9) adalah lebih rendah berbanding dengan DSSC berasaskan TiO₂ sahaja (4.09%). Ini adalah disebabkan oleh kadar rekombinasi yang lebih tinggi akibat daripada pinggir jalur konduksi SnO₂ yang lebih rendah berbanding dengan TiO₂. Walau bagaimanapun, kecekapan sel ini adalah 2 dan 71 kali lebih tinggi berbanding dengan SnO₂ sahaja (1.61%) dan Sn-MOF sahaja (0.05%) masing-masing. Muatan pewarna daripada fotoanod mendedahkan bahawa fotoanod SnO₂/TiO₂ (1:9) mempunyai kapasiti penjerapan pewarna yang tertinggi dalam kalangan fotoanod dengan kepekatan sebanyak 9.14×10^{-8} mol cm⁻². Ini menunjukkan bahawa fotoanod SnO₂/TiO₂ (1:9) boleh memberikan prestasi yang lebih baik daripada TiO₂ sahaja sekiranya rekombinasi dalam sel suria ini boleh disekat. Kajian ini telah memberikan pemahaman baharu terhadap fabrikasi fotoanod DSSC yang berprestasi tinggi.

TABLE OF CONTENTS

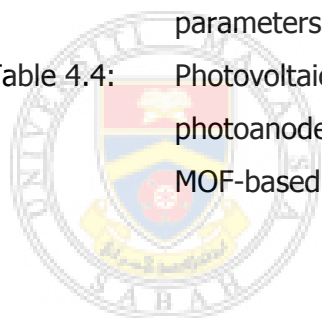
	Page
TITLE	i
DECLARATION	ii
CERTIFICATION	iii
ACKNOWLEDGEMENTS	iv
ABSTRACT	v
<i>ABSTRAK</i>	vi
TABLE OF CONTENTS	vii
LIST OF TABLES	x
LIST OF FIGURES	xi
LIST OF SYMBOLS AND ABBREVIATIONS	xiv
LIST OF APPENDICES	xvii
CHAPTER 1: INTRODUCTION	1
1.1 Dye-Sensitized Solar Cell Technologies and its Challenges	1
1.2 Objectives	4
1.3 Scope of Work	5
CHAPTER 2: LITERATURE REVIEW	6
2.1 Solar Cells	6
2.1.1 Background of Solar Cells	6
2.1.2 Classifications of Solar Cells	8
2.2 Dye-Sensitized Solar Cells (DSSCs)	15
2.2.1 Working Principles of DSSCs	15
2.2.2 Components of DSSCs	17

2.2.3	Photovoltaic Parameters for Evaluation of DSSC Performance	21
2.3	Metal-Organic Frameworks (MOFs)	24
2.3.1	Properties of MOFs	25
2.3.2	Synthetic Methods of MOFs	28
2.3.3	Activation of MOFs	34
2.3.4	MOF-Derived Materials	35
2.3.5	Photovoltaic Applications of MOFs	38
2.4	Tin Dioxide (SnO ₂)	44
2.4.1	Synthetic Methods of SnO ₂	45
2.4.2	Photovoltaic Applications of SnO ₂	46
CHAPTER 3: METHODOLOGY		51
3.1	Materials	51
3.2	Synthesis of Sn-MOF-Derived SnO ₂ Powder	52
3.3	Preparation of Sn-MOF-Derived SnO ₂ /TiO ₂ Powder Mixture	52
3.4	Fabrication of Dye-Sensitized Solar Cells (DSSCs)	53
3.5	Characterization of Sn-MOF-Derived SnO ₂ /TiO ₂ Photoanodes	55
3.5.1	Phase Identification of Sn-MOF-Derived SnO ₂ /TiO ₂ Photoanodes	55
3.5.2	Chemical Functionality of Sn-MOF-Derived SnO ₂ /TiO ₂ Photoanodes	56
3.5.3	Morphology of Sn-MOF-Derived SnO ₂ /TiO ₂ Photoanodes	56
3.5.4	Dye Loading of Sn-MOF-Derived SnO ₂ /TiO ₂ Photoanodes	57
3.5.5	Thickness of Sn-MOF-Derived SnO ₂ /TiO ₂ Photoanodes	59
3.6	Characterization of DSSCs	60
CHAPTER 4: RESULTS AND DISCUSSIONS		61

4.1	Characterization of Sn-MOF and Sn-MOF-Derived SnO ₂	61
4.1.1	Phase Identification of Sn-MOF and Sn-MOF-Derived SnO ₂	61
4.1.2	Chemical Functionality of Sn-MOF and Sn-MOF-Derived SnO ₂	62
4.1.3	Morphology of Sn-MOF and Sn-MOF-Derived SnO ₂	63
4.2	Characterization of Sn-MOF-Derived SnO ₂ /TiO ₂ Photoanodes	64
4.2.1	Phase Identification of Sn-MOF-Derived SnO ₂ /TiO ₂ Photoanodes	64
4.2.2	Chemical Functionality of Sn-MOF-Derived SnO ₂ /TiO ₂ Photoanodes	65
4.2.3	Morphology of Sn-MOF-Derived SnO ₂ /TiO ₂ Photoanodes	66
4.2.4	Dye Loading of Sn-MOF-Derived SnO ₂ /TiO ₂ Photoanodes	68
4.2.5	Thickness of Sn-MOF-Derived SnO ₂ /TiO ₂ Photoanodes	70
4.3	Photovoltaic Performances of Sn-MOF-Derived SnO ₂ /TiO ₂ Photoanodes	72
4.3.1	Current Density–Voltage Characteristics of Sn-MOF Photoanodes	72
4.3.2	Current Density–Voltage Characteristics of Sn-MOF-Derived SnO ₂ /TiO ₂ Photoanodes	74
CHAPTER 5: CONCLUSION AND FUTURE STUDIES		82
5.1	Conclusion	82
5.2	Future Studies	83
REFERENCES		84
APPENDICES		101

LIST OF TABLES

	Page
Table 2.1: Photovoltaic parameters of solar cells assembled using MOF-based materials at 100 mW cm^{-2}	39
Table 2.2: Photovoltaic parameters of DSSCs assembled using SnO_2 -based materials at 100 mW cm^{-2}	47
Table 3.1: Composition of Sn-MOF-derived $\text{SnO}_2/\text{TiO}_2$ powder mixture	53
Table 4.1: Dye adsorption of Sn-MOF-derived $\text{SnO}_2/\text{TiO}_2$ photoanodes	70
Table 4.2: Photovoltaic parameters of DSSC assembled using Sn-MOF photoanode at 60 mW cm^{-2} . The parameters of the best cells are highlighted in bold	73
Table 4.3: Photovoltaic parameters of DSSCs assembled using Sn-MOF-derived $\text{SnO}_2/\text{TiO}_2$ photoanodes at 60 mW cm^{-2} . The parameters of the best cells are highlighted in bold	75
Table 4.4: Photovoltaic parameters of DSSCs assembled using photoanodes of $\text{SnO}_2/\text{TiO}_2$ (1:9), SnO_2 -based materials, and MOF-based materials	80



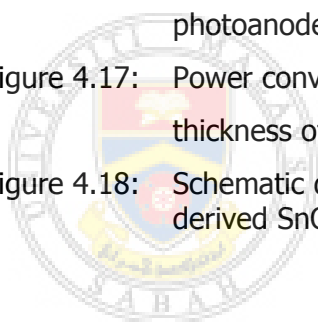
UMS
UNIVERSITI MALAYSIA SABAH

LIST OF FIGURES

	Page
Figure 2.1: Schematic illustrations of air mass with their corresponding zenith angle	7
Figure 2.2: Progress of best efficiencies recorded for certified solar cells	8
Figure 2.3: Device configuration of a CdTe solar cell	10
Figure 2.4: Device configuration of a CIGS solar cell	11
Figure 2.5: Operating principles and device configuration of an organic solar cell	12
Figure 2.6: Schematic illustrations of a typical DSSC	14
Figure 2.7: (a) Crystal structure of perovskite. Large cation A, blue spheres; small cation B, gray spheres; halide ion, purple spheres. (b) Device configuration of a perovskite solar cell	15
Figure 2.8: Operating principles of a DSSC	16
Figure 2.9: Kinetic data for the electron transfer processes in a DSSC	17
Figure 2.10: Schematic diagrams of DSSC device before and after the introduction of light scattering layer	18
Figure 2.11: Ruthenium-based dye sensitizers N3, N719, and black dye. TBA = tetra-n-butylammonium	19
Figure 2.12: Schematic illustration of a J–V curve	22
Figure 2.13: Schematic diagrams of MOF-5 ($[\text{Zn}_4\text{O}(\text{BDC})_3]_n$) (top) and HKUST-1 ($[\text{Cu}_3\text{O}(\text{BTC})_2]_n$) (bottom) framework. The combination of the inorganic units and organic linkers give rise to the formation of a MOF	24
Figure 2.14: Schematic illustrations of the formation of hollow Co_3O_4 dodecahedron: (a) ball-in-dodecahedron and (b) concave-dodecahedron	38
Figure 2.15: (a) Schematic illustration of MOF-5-derived ZnO parallelepipeds as scattering layer in DSSC. (b) J-V curves of devices assemble using ZnO (cell 1), MOF-5-derived ZnO/ZnO (cell 2) and ZIF-8/MOF-5-derived ZnO/ZnO (cell 3)	40
Figure 2.16: The bulk structures of several SnO_2 polymorphs	45

Figure 2.17:	(a) Schematic diagram of the pathway of electron in SnO ₂ /rGO-based DSSC. (b) Energy level diagram of DSSC assembling using SnO ₂ /rGO	50
Figure 3.1:	Schematic illustration of the synthesis of Sn-MOF-derived SnO ₂ powder	52
Figure 3.2:	Schematic illustration of the fabrication of DSSCs	54
Figure 3.3:	X-ray diffractometer Philips X'Pert Pro PW 3040	55
Figure 3.4:	Perkin-Elmer Spectrum 100 Spectrometer	56
Figure 3.5:	Scanning Electron Microscope JEOL JSM-5610LV	57
Figure 3.6:	Agilent Cary 60 UV-Vis spectrophotometer	58
Figure 3.7:	Surface Profilometer NanoMap 500LS	59
Figure 3.8:	Potentiostat Autolab PGSTAT101 with a 60 W metal halide lamp	60
Figure 4.1:	PXRD pattern of Sn-MOF and Sn-MOF-derived SnO ₂	62
Figure 4.2:	FTIR spectra of Sn-MOF and Sn-MOF derived SnO ₂	63
Figure 4.3:	SEM images of Sn-MOF (a, b) and Sn-MOF-derived SnO ₂ (c, d)	64
Figure 4.4:	PXRD pattern of powders scraped from the photoanode after calcination	65
Figure 4.5:	FTIR spectra of powders scraped from the photoanode after calcination	66
Figure 4.6:	SEM images of photoanodes after calcination: (a) TiO ₂ , (b) SnO ₂ /TiO ₂ (1:9), (c) SnO ₂ /TiO ₂ (1:3), (d) SnO ₂ /TiO ₂ (1:1), (e) SnO ₂ /TiO ₂ (3:1), and (f) SnO ₂	67
Figure 4.7:	Photographs of photoanodes after dye-sensitization: (a) TiO ₂ , (b) SnO ₂ /TiO ₂ (1:9), (c) SnO ₂ /TiO ₂ (1:3), (d) SnO ₂ /TiO ₂ (1:1), (e) SnO ₂ /TiO ₂ (3:1), and (f) SnO ₂	69
Figure 4.8:	UV-Vis absorption spectra of dyes desorbed from the Sn-MOF-derived SnO ₂ /TiO ₂ photoanodes	69
Figure 4.9:	Cross-sectional SEM images photoanodes after calcination: (a) TiO ₂ , (b) SnO ₂ /TiO ₂ (1:9), (c) SnO ₂ /TiO ₂ (1:3), (d) SnO ₂ /TiO ₂ (1:1), (e) SnO ₂ /TiO ₂ (3:1), and (f) SnO ₂ . The green line indicates the thickness of the film	71

Figure 4.10:	Trends of photoanode thickness with increasing loading of Sn-MOF-derived SnO ₂ . The thickness of photoanodes was measured using profilometer and SEM	72
Figure 4.11:	J–V curve of DSSC assembled using Sn-MOF photoanode at 60 mW cm ⁻²	73
Figure 4.12:	J–V curve of DSSC assembled using Sn-MOF photoanode in dark	74
Figure 4.13:	J–V curves of DSSCs assembled using Sn-MOF-derived SnO ₂ /TiO ₂ photoanodes at 60 mW cm ⁻²	75
Figure 4.14:	J–V curves of DSSCs assembled using Sn-MOF-derived SnO ₂ /TiO ₂ photoanodes in dark	76
Figure 4.15:	Trends of V _{oc} and J _{sc} with different loading of Sn-MOF-derived SnO ₂	78
Figure 4.16:	Power conversion efficiencies of DSSCs assembled using photoanodes of Sn-MOF-derived SnO ₂ /TiO ₂ and Sn-MOF	79
Figure 4.17:	Power conversion efficiencies of DSSCs as a function of thickness of photoanodes	80
Figure 4.18:	Schematic diagram of DSSC assembled using Sn-MOF-derived SnO ₂ /TiO ₂ photoanode	81



UMS
UNIVERSITI MALAYSIA SABAH

LIST OF SYMBOLS AND ABBREVIATIONS

AC	-	Alternating current
AIPV	-	Automobile integrated photovoltaic
AM	-	Air mass
ATR	-	Attenuated total reflectance
BASF	-	Badische Anilin- und Soda-Fabrik
BDC	-	1,4-benzenedicarboxylate
BET	-	Brunauer-Emmett-Teller
BHJ	-	Bulk heterojunction
BIPV	-	Building integrated photovoltaic
BTC	-	1,3,5-benzenetricarboxylate
c	-	Concentration of dye
CIGS	-	Copper indium (gallium) diselenide
CZO	-	Cobalt-doped zinc oxide
DABCO	-	1,4-diazabicyclo[2.2.2]octane
DC	-	Direct current
DSSC	-	Dye-sensitized solar cell
DUT	-	Dresden University of Technology
2-EtIm	-	2-ethylimidazole
EQE	-	External quantum efficiency
FF	-	Fill factor
FTIR	-	Fourier transform infrared spectroscopy
FTO	-	Fluorine-doped tin oxide
hier-TiO₂	-	Hierarchical anatase titanium(IV) oxide
H₂BDC	-	1,4-benzenedicarboxylic acid
H₃BTC	-	1,3,5-benzenetricarboxylic acid
HKUST	-	Hong Kong University of Science and Technology
HOMO	-	Highest occupied molecular orbital
Im	-	Imidazole
IMPS	-	Intensity-modulated photocurrent spectroscopy
IMVS	-	Intensity-modulated photovoltage spectroscopy
INA	-	Isonicotinic acid

IPCE	-	Incident photon to current conversion efficiency
IRMOF	-	Isorecticular metal-organic framework
IUPAC	-	International Union of Pure and Applied Chemistry
I_{sc}	-	Short circuit current
I–V	-	Current–voltage
ITO	-	Indium tin oxide
J_{sc}	-	Short circuit current density
J–V	-	Current density–voltage
l	-	Path length of light beam
LAG	-	Liquid-assisted grinding
LBL	-	Layer-by-layer
LHE	-	Light harvesting efficiency
LIB	-	Lithium ion battery
LUMO	-	Lowest unoccupied molecular orbital
MB	-	Methylene blue
2-MeIm	-	2-methylimidazole
mesoMOF	-	Mesoporous metal-organic framework
meso-SnO₂	-	Mesoporous tin(IV) oxide
MIL	-	Matériaux de l'Institut Lavoisier
MOF	-	Metal-organic framework
MWCNT	-	Multi-walled carbon nanotube
nc-TiO₂	-	Nanocrystalline titanium(IV) oxide
NDC	-	2,6-naphthalenedicarboxylate
NTE	-	Negative thermal expansion
OLED	-	Organic light-emitting diode
PCE	-	Power conversion efficiency
PCP	-	Porous coordination polymer
PEBII	-	Poly((1-(4-ethenylphenyl)methyl)-3-butyl-imidazolium iodide)
PEDOT	-	Poly(3,4-ethylenedioxythiophene)
PEGDA	-	Polyethylene glycol diacrylate
PEGDGE	-	Poly(ethylene glycol) diglycidyl ether
PEGMA	-	Poly(ethylene glycol) methyl ether methacrylate

P_{in}	-	Intensity of incident light
P_{max}	-	Maximum power
PSS	-	Poly(styrene sulfanate)
Pt	-	Platinum
PV	-	Photovoltaic
PXRD	-	Powder X-ray diffractometry
rGO	-	Reduced graphene oxide
Ru	-	Ruthenium
scCO₂	-	Supercritical carbon dioxide
SEM	-	Scanning electron microscopy
ssDSSC	-	Solid-state dye-sensitized solar cell
4-tbp	-	4- <i>tert</i> -butylpyridine
TEA	-	Triethylamine
TEM	-	Transmission electron microscopy
QD	-	Quantum dot
UMCM	-	University of Michigan Crystalline Material
UV	-	Ultraviolet
V_{oc}	-	Open circuit voltage
ZIF	-	Zeolitic imidazolate framework
η	-	Power conversion efficiency
λ	-	Wavelength
ϕ	-	Incident radiative light flux
ϕ_{inj}	-	Quantum yield for the electron injection
η_{coll}	-	Electron collection efficiency
μ_e	-	Electron mobility
ϵ	-	Molar extinction coefficient

LIST OF APPENDICES

	Page
Appendix A Calibration curve of N719 dye in 0.1 M NaOH solution in a mixed solvent of water and ethanol (1:1 v/v)	101
Appendix B FTIR spectrum of terephthalic acid condensed phase from Sigma-Aldrich	102
Appendix C UV-Vis absorption data of Sn-MOF-derived SnO ₂ /TiO ₂ photoanodes	103



UMS
UNIVERSITI MALAYSIA SABAH

CHAPTER 1

INTRODUCTION

1.1 Dye-Sensitized Solar Cell Technologies and its Challenges

Fossil fuels are currently the global largest energy source which accounts for over 80% of the present energy (Yu *et al.*, 2012). However, fossil fuel may not be able to fulfill the daily energy demand of human in future due to the increasing energy demands and depletion of fossil fuels. This may lead to serious energy crisis in the near future and has motivated in the use of renewable energy as alternative to fossil fuel. The field of renewable energy has become of great interest to fulfill the rapid growing of power needs. The renewable energy has been considered as the fastest growing energy sources that generate electricity at 3.4% per year from 2008 to 2035 (Tetreault and Gratzel, 2012). Solar energy has been regarded as the most promising alternative to fossil fuel among the renewable energy sources. The energy from radiation of Sun in an hour is equivalent to the global energy needs in one year. Unfortunately, the solar energy only constitutes 0.04% of the current world energy (Wang *et al.*, 2012).

The present photovoltaic technologies were dominated by the first and second generation solar cells. The first generation solar cells are mainly consist of monocrystalline and multicrystalline silicon solar cells. However, these solar cells are suffered from complexity in manufacturing and expensive fabrication cost. The second generation solar cells are thin film solar cells. These solar cells have a cheaper fabrication cost but recorded a lower efficiencies than the silicon-based solar cells. Third generation solar cells are emerging photovoltaic technologies that aiming to achieve both low cost fabrication and high efficiency (Hu *et al.*, 2010; Yu *et al.*, 2012). Among the third-generation photovoltaic technologies, dye-sensitized

solar cell (DSSC) stands out as one of the most attractive candidates for the next-generation solar cell.

DSSC is a promising alternative to conventional silicon-based solar cells owing to their low fabrication cost, high efficiency and environmentally friendly (Hagfeldt *et al.*, 2010; Thomas *et al.*, 2014). Since the pioneering work by O'Regan and Grätzel in 1991, nanocrystalline titanium(IV) oxide (TiO₂)-based photoanode have been studied extensively due to its high photovoltaic performance (O'Regan and Grätzel, 1991). Up to now, the highest power conversion efficiency of DSSC was achieved at 13% on a laboratory scale (Mathew *et al.*, 2014). Over the past decade, DSSC has been introduced in applications such as indoor electronic appliances, shaded conditions and cloudy weather. Their transparency and variety of colours also make them preferable for applications in building integrated photovoltaics (BIPVs) and automobile integrated photovoltaics (AIPVs) (Wali *et al.*, 2015a).

A DSSC typically consists of a dye-sensitized semiconducting layer on fluorine-doped tin oxide (FTO) glass as photoanode, I⁻/I₃⁻ based liquid electrolyte and a platinized FTO glass as counter electrode (Roy-Mayhew and Aksay, 2014). One of the most crucial components in DSSC is photoanode as it responsible for anchoring the dye molecules and the separation of charge carriers. TiO₂ semiconductor is usually used to construct photoanode in DSSC due to its wide bandgap (~3.2 eV) and higher conduction band edge energy (Hagfeldt *et al.*, 2010). However, TiO₂ suffers from the charge recombination at the TiO₂/dye and TiO₂/electrolyte interfaces which hinders their practical application in DSSCs (Li *et al.*, 2011). Hence, there is a great need to modify the TiO₂ photoanode to improve the electron transport in DSSCs.

SnO₂ is an n-type semiconductor which is widely used in applications such as transparent conducting electrodes, heterogeneous catalysis, solar cells, gas sensors, *etc* (Batzill and Diebold, 2005). It is one of the earliest semiconductors that have been applied in DSSC. It has been considered as another great option for the photoanode of DSSC due to its high electron mobility and larger energy

bandgap (~ 3.6 eV). Nevertheless, it has low isoelectric point (pH 4–5) and poor dye adsorption (Wali *et al.*, 2015a). Thus, SnO₂ cannot be applied directly as photoanode and modification is needed for its application in DSSC.

Metal-organic frameworks (MOFs), also known as porous coordination polymers (PCPs), are crystalline nanoporous materials composed of metal ions or clusters as nodes with organic ligands as linkers (Furukawa *et al.*, 2013). MOFs have been widely investigated in applications such as gas storage, separation, catalysis, drug delivery, and sensing owing to their tunable pore size, high surface area, and high porosity (Rowsell and Yaghi, 2004). Currently, applications of MOFs in DSSCs are still in its infancy and the direct use of MOFs as active material in DSSC is rare (Li *et al.*, 2014b).

In 2011, Wei and co-workers for the first time introduced MOF as an interfacial modifier to improve the open circuit voltage (V_{oc}) of DSSC. They coated a layer of ZIF-8 on nanocrystalline TiO₂ layer of photoanode and recorded a high conversion efficiency of 5.34% for their DSSC device (Li *et al.*, 2011). MOFs are regarded as potential candidates for photoanode in DSSC due to their flexible fabrication and permanent porosity (Li *et al.*, 2011). Nevertheless, majority of MOFs have insulating behaviour which are detrimental to the transport of electrons across the cell and subsequently lead to poor performance DSSC device (Lee *et al.*, 2014d).

Recently, MOFs have been employed as sacrificial template or precursor to obtain porous carbon or metal oxides under thermolysis conditions (Sun and Xu, 2014). These MOF-derived materials have become a popular topic for applications in energy conversion and storage. For instance, MOF-derived metal oxides have been shown to exhibit a better electrical conductivity and better thermal stability compared to MOFs. These unique properties make them a great option for improving the photoanode of DSSCs. In 2014, Wei and co-workers developed MOF-5-derived ZnO parallelepipeds as light scattering layer for ZnO photoanode of DSSC and reported a power conversion efficiency of 3.67% (Li *et al.*, 2014a). In another study, the same group prepared hierarchical anatase TiO₂-based

photoanode by using titanium MOF MIL-125 as sacrificial template. The device recorded a high efficiency of 7.20%, which is higher than that of P25 (6.37%) (Dou *et al.*, 2016). Hence, MOF-derived metal oxide could be couple with TiO₂ for preparation of photoanode with enhanced photovoltaic performance.

In this study, Sn-MOF-derived SnO₂ was loaded into nanocrystalline TiO₂ photoanode to improve the overall photovoltaic performance of the DSSC devices. To date, there are only few studies on the fabrication of photoanode consisting of SnO₂ and TiO₂ in the application of DSSCs. Sn-MOF-derived SnO₂/TiO₂ powder mixture was prepared by direct mixing of as-synthesized Sn-MOF-derived SnO₂ and commercial TiO₂ (P25). The mixture was then fabricated onto FTO glass substrate by doctor-blade method and employed as photoanode of DSSC. These Sn-MOF-derived SnO₂/TiO₂ photoanodes were then characterized using PXRD, FTIR, and SEM. UV-Vis spectrophotometer was employed to investigate the dye loading on the Sn-MOF-derived SnO₂/TiO₂ photoanodes. The thickness of photoanodes was measured using profilometer and SEM.

To the best of our knowledge, there has been no report on the loading of Sn-MOF-derived SnO₂ into TiO₂ photoanode of DSSC. This is the first time Sn-MOF-derived SnO₂/TiO₂ powder mixture was applied as photoanode in DSSC. The synergistic interactions between SnO₂ and TiO₂ improve the dye loading on the photoanodes and enhance the electron transport across the cell. The power conversion efficiencies (PCEs) of DSSCs assembled using the Sn-MOF-derived SnO₂/TiO₂ photoanodes were investigated using potentiostat under illumination of 60 mW cm⁻². This work could provide a new insight on the applications of Sn-MOF-derived SnO₂ photoanode in DSSC.

1.2 Objectives

The objectives of this research are:

- (i) To prepare Sn-MOF-derived SnO₂/TiO₂ photoanodes with varying weight ratio through doctor-blade method,

- (ii) To characterize Sn-MOF-derived SnO₂/TiO₂ photoanodes using PXRD, FTIR, SEM, and profilometer,
- (iii) To investigate the dye loading of Sn-MOF-derived SnO₂/TiO₂ photoanodes using UV-Vis spectrophotometer, and
- (iv) To evaluate the power conversion efficiency of dye-sensitized solar cells assembled using Sn-MOF-derived SnO₂/TiO₂ photoanodes.

1.3 Scope of Work

This research focuses on the assembly of dye-sensitized solar cells (DSSCs) using Sn-MOF-derived SnO₂/TiO₂ photoanode. The works involve the preparation of Sn-MOF powder, Sn-MOF-derived SnO₂ powder, and Sn-MOF-derived SnO₂/TiO₂ powder mixture, followed by characterization of the materials and photoanode using powder X-ray diffractometry (PXRD), Fourier transform infrared spectroscopy (FTIR), scanning-electron microscopy (SEM), UV-Vis spectrophotometer, and surface profilometer. The Sn-MOF-derived SnO₂/TiO₂ photoanode, for instance, was immersed in N719 ethanolic dye solution before the assembly of DSSCs. The power conversion efficiency of DSSCs assembled using Sn-MOF-derived SnO₂/TiO₂ photoanode was measured using potentiostat under simulated illumination of 60 mW cm⁻².

CHAPTER 2

LITERATURE REVIEW

2.1 Solar Cells

2.1.1 Background of Solar Cells

The global energy consumption is expected to double to 30 TW by 2050 and triple to 46 TW by the end of this century (Lewis and Crabtree, 2005). Fossil fuels are the main energy source in present and contribute about 80% of the global energy (Yu *et al.*, 2012). The increase in energy demands and depletion of fossil fuels have driven the search for a new energy as alternative energy to fossil fuels. Renewable energy sources such as wind, solar, and nuclear emerged as a potential alternative owing to their environmental friendliness and readily available. Solar energy emerged as a promising renewable energy to fulfill the needs. It has attracted much attention due to its availability, low cost, and clean energy. Solar farms with an efficiency of 10% could generate about 60 TW of power (Hagfeldt *et al.*, 2010).

Sun is the most abundant energy on Earth and it emits light with wavelength ranging from ultraviolet to visible and to infrared (Hagfeldt *et al.*, 2010). As the solar radiation passes through the atmosphere, it is partially absorbed by gases of low concentration in the infrared region. The absorption of solar radiation increases with the path length through the atmosphere and the mass of air during its passage through the atmosphere (Würfel, 2005). Air mass (AM) refers to the shortest path length through the atmosphere of the maximum radiation that strikes the surface of Earth at the zenith when the skies are clear. AM can be defined as $AM = 1/\cos \phi$ where ϕ is the elevation angle of the sun (Hagfeldt *et al.*, 2010). AM 0 corresponds to the extraterrestrial spectrum which is